Silica-Based Planar Lightwave Circuits for WDM Applications

Katsunari Okamoto, Yasuyuki Inoue, Takuya Tanaka and Yasuji Ohmori

NTT Opto-electronics Laboratories

162 Tokai, Ibaraki, 319-11, Japan

Summary

Planar lightwave circuits (PLCs) provide various important devices for optical wavelength division multiplexing (WDM) systems, subscriber networks and etc. This paper reviews the recent progress and future prospects of PLC technologies including arrayed-waveguide grating multiplexers, optical add/drop multiplexers, programmable dispersion equalizers and hybrid optoelectronics integration technologies.

key words : silica waveguide, planar lightwave circuits, arrayed-waveguide grating multiplexer, optical add/drop multiplexer, and WDM

1. Introduction

A variety of passive PLCs such as NxN star couplers, thermo-optic matrix switches and NxN arrayed-waveguide grating (AWG) multi/demultiplexers for WDM systems have been fabricated [1] - [3]. The most prominent feature of the silica waveguides is their simple and well defined waveguide structures. This allows us to fabricate spatial multi-beam or temporal multi-stage interference devices. Hybrid opto-electronics integration based on the terraced-silicon platform technologies have also been developed both for the fiber-to-the-home (FTTH) applications and high-speed signal processings [4], [5].

Planar lightwave circuits using silica-based optical waveguides are fabricated on silicon or silica substrate by a combination of flame hydrolysis deposition (FHD) and reactive ion etching (RIE). Fine glass particles are produced in the oxy-hydrogen flame and deposited on substrates. After depositing under-cladding and core glass layers, the wafer is heated to high temperature for consolidation. The circuit pattern is fabricated by photolithography and reactive ion etching. Then core ridge structures are covered with over-cladding layer and consolidated again.

The typical bending radius R of silica waveguide is around 2 mm ~ 15 mm. Therefore the chip size of the large-scale integrated circuit becomes several centimeters square. The propagation loss reduction and the uniformity of refractive index and core geometry throughout the wafer are strongly required. Propagation loss of 0.1 dB/cm was obtained in a 2-m long waveguide with $\Delta = 2\%$ index difference (R=2mm) [6] and loss of 0.035 dB/cm was obtained in a 1.6-m long waveguide with $\Delta = 0.75\%$ index difference (R=5mm) [7], respectively. Further loss reduction down to 0.017 dB/cm has been achieved in a 10-m long waveguide with $\Delta = 0.45\%$ index difference (R=15mm) [8].

2. Arrayed-Waveguide Grating

2.1. Principle of Operation

An NxN arrayed-waveguide grating (AWG) multiplexer is very attractive in optical WDM networks since it is capable of simultaneously processing N^2 optical channels at N different wavelengths [9],[10]. The arrayed-waveguide grating consists of input/output waveguides, two focusing slab regions and a phase-array of multiple channel waveguides with the constant path length difference ΔL between neighboring waveguides (Fig. 1). The input light is radiated to the first slab and then excites the arrayed channel waveguides. After traveling through the arrayed waveguides, the light beams constructively interfere into one focal point in the second slab. The location of this focal point depends on the signal wavelength since the relative phase delay in each waveguide is given by $\Delta L/\lambda$. The dispersion of the focal position x with respect to the wavelength λ is given by

$$\frac{\triangle X}{\triangle \lambda} = -\frac{N_c f \triangle L}{n_s d \lambda_0} \quad (1)$$

where f is the focal length of the converging slab, n_s is the effective index in the slab region, N_c is the group index of the effective index n_c of the array waveguide ($N_c = n_c - \lambda dn_c/d\lambda$), d is the pitch of the array waveguides at slab-array interface and λ_o is the center wavelength of WDM signals, respectively. The diffraction order m is given by $m = n_c \triangle L/\lambda_0$. The spacial separation of the m-th and (m+1)-th focused beams for the same wavelength is expressed as

$$X_{FSR} = x_m - x_{m+1} = \frac{\lambda_0 f}{n_s d} \quad (2)$$

X_{FSR} represents the free spacial range of AWG.. Number of available wavelength channels N_{ch} is given by dividing X_{FSR} with the output waveguide separation D as

$$N_{ch} = \frac{X_{FSR}}{D} = \frac{\lambda_0 f}{n_s d D} \quad (3)$$

When center wavelength λ_0 and number of channels N_{ch} in WDM system are given, arc radius f of the slab region is determined by Eq.

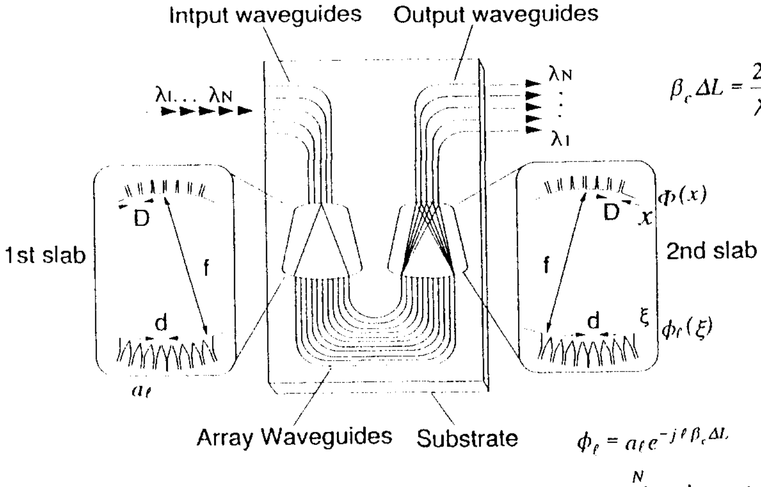

$$\beta_c \Delta L = \frac{2\pi}{\lambda_0} n_c \Delta L = 2m\pi$$

$$\phi_\ell = a_\ell e^{-j\ell\beta_c \Delta L}$$

$$\Phi(x) = \sum_{\ell=1}^{N} \mathcal{F}\{\phi_\ell\} = \mathcal{F}\{\sum_{\ell=1}^{N} \phi_\ell\} = \mathcal{F}\{\phi(\xi)\}$$

Fig. 1. Schematic configuration of arrayed- waveguide grating multiplexer.

(3), where waveguide parameters n_s, d and D are already known. The separation of the focal positions should be $|\triangle x| = D$ for the WDM signals with wavelength spacing $\triangle\lambda$. Therefore path length difference $\triangle L$ is obtained from Eq. (1) as

$$\triangle L = \frac{n_s d D \lambda_0}{N_c f \triangle\lambda} \quad (4)$$

The electric field profile $\Phi(x)$ at the output plane of AWG (Fig. 4) is the summation of the farfield patterns Φ_ℓ's from each array waveguide. Therefore, $\Phi(x)$ is the summation of the spatial Fourier transforms of Φ_ℓ's. We can exchange summation and Fourier transformation in the linear system. Then it is shown that the focused electric field profile $\Phi(x)$ at the output is the Fourier transform of the entire electric field profile $\Phi(\xi)$ at slab-array interface.

We have fabricated various kinds of multiplexers ranging from 50-nm spacing 8-channel AWG to 50-GHz spacing 64-channel AWGs (Fig. 2) [11]. Table I shows experimental and theoretical performances of several kinds of AWG multiplexers. In all of these practical AWGs, crosstalks of about -30 dB have been obtained. Numbers in parentheses are the designed values ($\lambda_0 s$) and calculated values (3 dB bandwidths) by BPM, respectively. Experimental results agree well with the theoretical values. Multiplexers with narrower channel spacing exhibited much higher (worse) crosstalks due to the phase errors in array waveguides. We have succeeded in fabrication of 128×128 AWG with 25-GHz channel spacing by improving the core deposition conditions [12]. Figure 3 shows the demultiplexing properties for the entire 128 output ports. The crosstalks to the neighboring channels are less than -16 dB and the on-chip loss ranges from 3.5 to 5.9 dB for central and peripheral output ports. If the sub-peaks near the pass bands are eliminated by the phase-error compensation techniques [13], crosstalks can be improved by about 10 dB down to -25 dB levels.

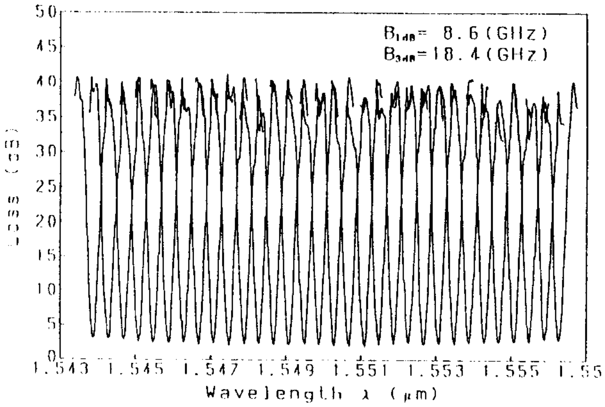

Fig. 2. Demultiplexing properties of central 32 channels in 64ch_50GHz spacing AWG.

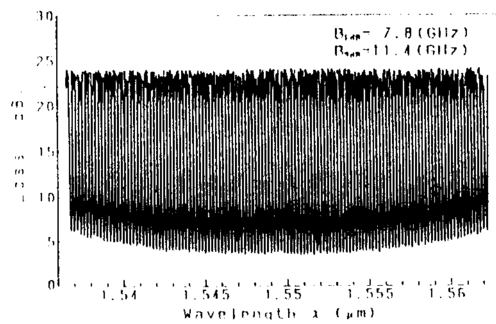

Fig. 3. Demultiplexing properties of 128ch_25GHz spacing AWG.

2.2. Flat Spectral Response AWG

Since the dispersion of the focal position x with respect to the wavelength λ is almost constant, the transmission loss of normal AWG monotonically increases around the center wavelength of each channel. This places tight restrictions on the wavelength tolerance of laser diodes and requires accurate temperature control for both AWGs and laser diodes. Moreover, since optical signals are transmitted through several filters in the WDM ring/bus networks, cumulative passband width of each channel becomes much narrower than that of the single-stage AWG filter. Therefore, flat and broadened spectral responses are required for AWG multiplexers. Several approaches have been proposed to flatten the pass bands of AWGs [14]-[16]. We proposed a flat-response AWG multiplexer having parabolic waveguide horns in the input waveguides [17].

Figure 4 shows the enlarged view of the interface between (a) input waveguides and first slab and (b) second slab and output waveguides, respectively. The width of the parabolic horn along the propagation direction z is given by [18]

$$W(z) = \sqrt{2\alpha\lambda_g z + (2\alpha)^2} \quad (5)$$

where α is a constant less than unity, λ_g is the wavelength in the guide ($\lambda g = \lambda / n_{eff}$) and 2α is the core width of the channel waveguide, respectively. At the proper horn length z=800μm, a slightly double-peaked flat intensity distribution can be obtained with the horn parameters of α=1 and 2α=7μm. The broadened and double-peaked field is imaged onto the entrance of an output waveguide having normal core width. The overlap integral of the refocussed field with the local normal mode of the output waveguide gives the flattened spectral response of AWG. Figure 5 shows the demultiplexing properties of 16ch-100GHz spacing AWG having parabolic horns with W=40μm and z=800μm. The crosstalks to the neighboring channels are less than -35 dB and the on-chip loss is about 7.0 dB. The average 1-dB, 3-dB and 20-dB bandwidths are 86.4 GHz, 100.6 GHz and 143.3 GHz, respectively.

It has been confirmed that in order to obtain a flat spectral response, it is necessary to produce the rectangular electic field profile at the focal plane (interface between the second slab and output waveguides). Since the electric field profile in the focal plane is the Fourier transform of the field in the array output aperture (interface between the array waveguide and second slab), such a rectangular field profile could be generated when the electric field at the array output aperture obeys a sin(ξ)/ξ distribution where ξ is measured along the array output aperture [14].

Figure 6 shows the electric field amplitude and relative phase delays (excess phase value added to

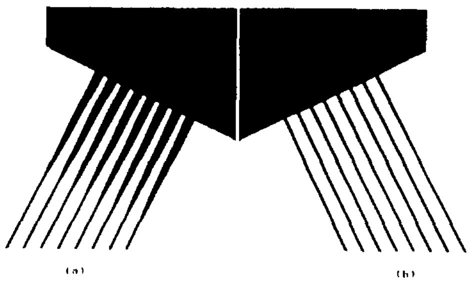

Fig. 4. Enlarged view of the interface between (a) input waveguides and first slab and (b) second slab and output waveguides in flat response AWG.

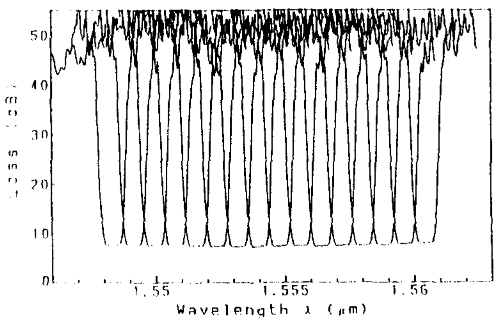

Fig. 5. Demultiplexing properties of 16ch_100GHz spacing AWG having parabolic horns with W=40 μm and z = 400 μm.

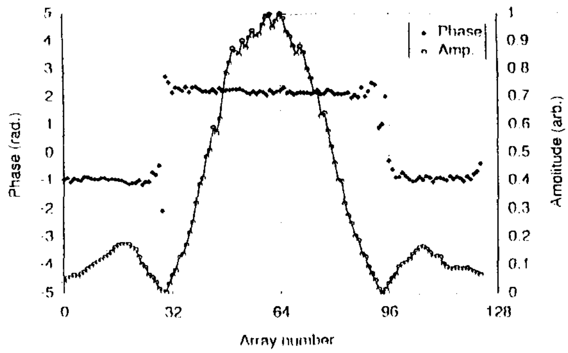

Fig. 6. Electric field amplitude and relative phase delays in the sinc-type flat response AWG.

I x $\triangle L$ where i denotes the the i-th array waveguide) in the sinc-type flat response AWG measured by the low coherence Fourier transform spectroscopy [19]. Sinc-shaped electric field distribution was realized by varying the core aperture width of the waveguide at the first slab-array interface. The excess path length differences of π for the negative sinc values were realized by the additional path length $\delta \ell = \lambda / 2n_c$ to the corresponding array waveguides. The crosstalk and flat passband characteristics are almost the same as those of parabola-type AWGs.

2.3. Uniform-Loss and Cyclic-Frequency (ULCF) AWG

It is well recognized that N x N signal interconnection in AWG can be achieved when free spectral range (FSR) of AWG is N times the channel spacing. Here FSR is given by

$$FSR = \frac{n_c \nu_0}{N_C m} \qquad (6)$$

where ν_0 is the center frequency of WDM signals. Light beams with three different diffraction orders of m-1, m and m+1 are utilized to achieve N x N interconnections [20]. Typical diffraction order is m=60 for 32-channel AWG with 100-GHz channel spacing as shown in Table I. Since FSR is inversely proportional to m, substantial center frequency mismatch is brought by the difference between three FSRs. Also insertion losses of AWG for peripheral input and output ports are 2~3 dB higher than those for central ports [2],[21]. These loss nonuniformity and noncyclic frequency characteristics in conventional AWGs are main obstacles which prevent the development of practical N x N routing networks. We have fabricated 32 x 32 arrayed-waveguide grating having uniform-loss and cyclic-frequency characteristics. Fig. 7 shows the schematic configuration of uniform-loss and cyclic-frequency (ULCF) arrayed-waveguide grating. It consists of 80-channel AWG multiplexer with 100-GHz spacing and 32 optical combiners which are connected to 72 output waveguides of the multiplexer. The arc length of slab is f and number of array waveguides is 300 having the constant path length difference $\triangle L$= 24.6μm between neighboring waveguides. The diffraction order is m=23 which gives a free spectral range of FSR=8THz. In the input side, 32 waveguides ranging from #25 to #56 are used for the input waveguides so as to secure the uniform loss characteristics [11]. In the output side, two waveguides ((i+8)-th and (i+40)-th waveguide for i=1~32) are combined through waveguide intersection and multimode interference (MMI) coupler to make one output port. Since the peripheral output ports are not used, uniform loss characteristics are obtained. The inset of Fig. 15 shows the principle how the ULCF arrayed-waveguide grating is constructed. In this example 4 x 4 ULCF AWG is fabricated from 10 x 10 original AWG. Multiplexed signals with wavelength λ_4, λ_5, λ_6, λ_7 which are coupled to input port #4 are demultiplexed into output waveguides from #5 to #8. When signals λ_4, λ_5, λ_6, λ_7 are coupled to input port #5, signal component λ_4 is folded back into output waveguide #8 through the optical combiner. This is the operational principle of the ULCF AWG.

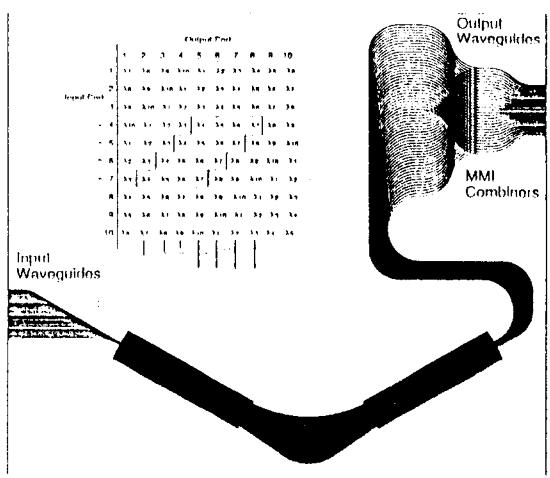

Fig. 7. Schematic configuration of uniform-loss and cyclic-frequency AWG.

Though we could improve the loss characteristics, we should pay at least 3-dB loss budget in optical combiners to achieve uniform loss and cyclic frequency characteristics. We first show the light splitting properties of the conventional 32-channel AWG with 100-GHz spacing [14]. Fig. 8(a) shows measured insertion losses for entire input/output combinations in the conventional AWG. The peak-to-peak loss variation is 4.7 dB (minimum loss α_{min}, maximum loss α_{max} = 7.8 dB) and the standard deviation is σ_{loss}. Fig. 8(b) shows deviations of the channel center frequency from the prescribed values. The peak-to-peak variation is 75.6 GHz ($\delta\nu_{min}$ = −44.5 GHz, $\delta\nu_{max}$ = 31.1 GHz) and the standard deviation is δ_{freq} = 16.7 GHz. Major reason for center frequency mismatch is the difference of FSR in neighboring diffraction orders. Figs. 9(a) and (b) show insertion losses and channel center frequency

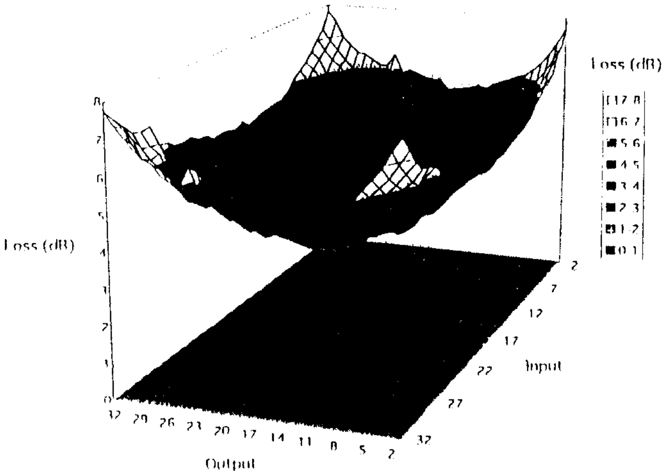

Fig. 8(a). Measured insertion losses for entire 32 x 32 input/output combinations in the conventional AWG.

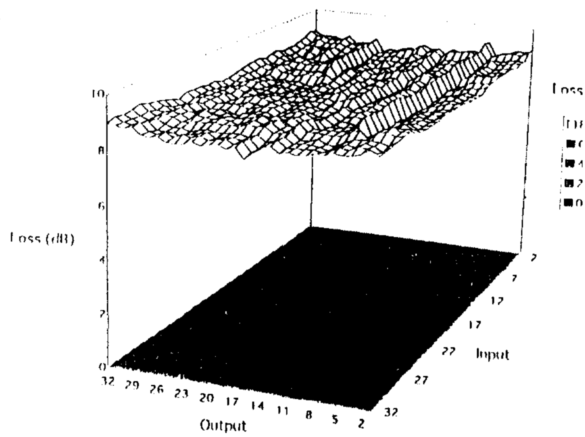

Fig. 9(a). Measured insertion losses for entire 32 x 32 input/output combinations in the uniform-loss and cyclic-frequency AWG.

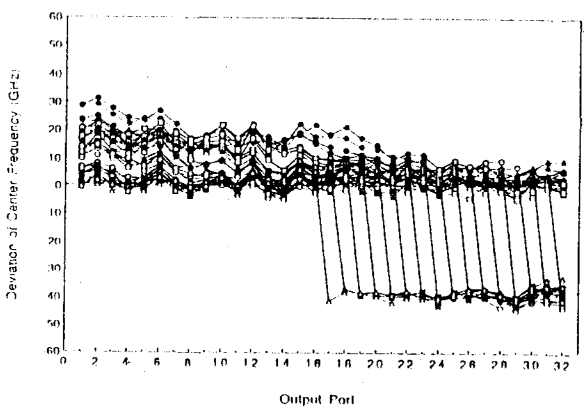

Fig. 8(b). Measured channel center frequency deviations for entire 32 x 32 input/output combinations in the conventional AWG.

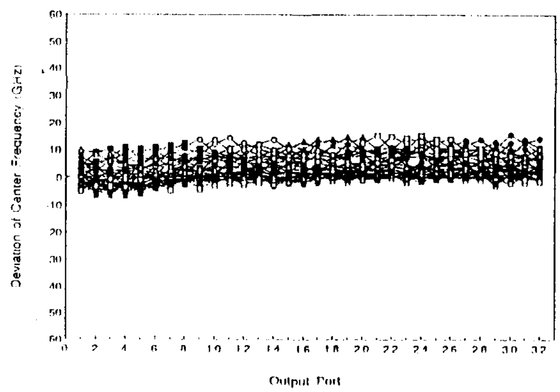

Fig. 9(b). Measured channel center frequency deviations for entire 32 x 32 input/output combinations in the uniform-loss and cyclic-frequency AWG.

deviations for 32-input/32-output combinations in the uniform-loss and cyclic-frequency AWG. The peak-to-peak loss variation is reduced to 1.2 dB (α_{min} = 8.1 dB, α_{max} = 9.3 dB) and the standard deviation is σ_{loss} = 0.2 dB. The peak-to-peak frequency variation is also reduced to 22.3 GHz ($\delta\nu_{min}$ = -6.8 GHz, $\delta\nu_{max}$ =15.5 GHz) and the standard deviation is σ_{freq} = 4.4 GHz. The crosstalk of the AWG is about -26 dB.

2.4. Athermal (Temperature Insensitive) AWG

Temperature sensitivity of the pass wavelength (frequency) in the silica-based AWG is about $d\lambda/dT$ = 1.2 x 10^{-2}(nm/deg) ($d\nu/dT$ = -1.5 (GHz/deg), which is mainly determined by the temperature dependence of silica glass itself ($dn_c/dT=1.1 \times 10^{-5}$(1/deg). The AWG multiplexer should be temperature controlled with a heater or a Peltier cooler to stabilize the channel wavelengths. This requires the constant power consumption of few watts and a lot of equipments for the temperature control. Recently, we have succeeded in fabrication of an athermal (temperature insensitive) AWG operating in the 0 - 85 ℃ temperature range [22]. Figure 10 shows a schematic configuration of athermal AWG. Temperature dependent optical path difference in silica waveguides is compensated with a triangular groove filled with silicone adhesive which has negative thermal coefficient. Since the pass wavelength is given by λ_0 = $n_c \Delta L/m$, optical path length difference $n_c \Delta L$ should be made insensitive to temperature. Therefore the groove is designed to satisfy the following conditions.

$$n_c \Delta L = n_c \Delta \ell + \hat{n}_c \Delta \hat{\ell} \qquad (7)$$

$$\frac{d(n_c \Delta L)}{dT} = \frac{d n_c}{dT} \Delta \ell + \frac{d \hat{n}_c}{dT} \Delta \hat{\ell} = 0 \qquad (8)$$

where $\hat{n}_c$ is the refractive index of silicone and $\Delta \ell$ and $\Delta \hat{\ell}$ are the path length differences of silica waveguides and silicone region. Eq. (7) is a condition to satisfy the AWG specifications and Eq. (8) is the athermal condition, respectively. The

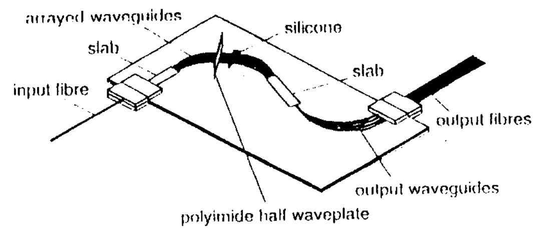

Fig. 10. Schematic configuration of athermal AWG.

temperature sensitivity of silicone is $d\hat{n}_c/dT$ = -37 x 10^{-5}(1/deg). Therefore the path length difference of silicone is $\Delta \hat{\ell} \cong \Delta \ell / 37$. Figure 11 shows temperature dependencies of pass wavelengths in conventional and athermal AWGs. The temperature dependent wavelength change has been reduced from 0.95 nm to 0.05 nm in the 0 - 85 ℃ range. The excess loss caused by the groove is about 2 dB which is mainly a diffraction loss. Figure 12 shows the loss change at 1552.52 nm during heat cycles from -40 to 85 ℃. The loss change is smaller than 0.2 dB. Furthermore, the channel wavelength change was less than 0.02 nm in a long-term test over 5000 hours at 75 ℃ and 90 % relative humidity.

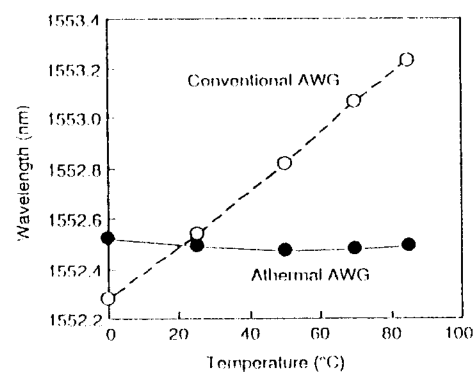

Fig. 11. Temperature dependences of pass wavelengths.

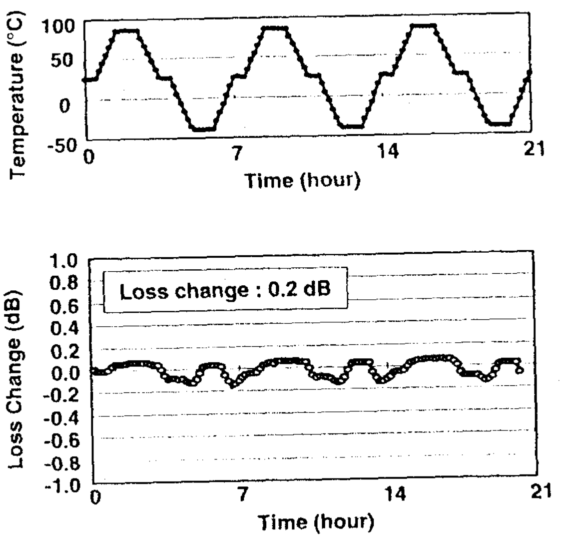

Fig. 12. Loss variation under heat cycle test from -40 to 85 ℃.

3. Optical Add/Drop Multiplexer

An optical add/drop multiplexer (ADM) is a device that gives simultaneous access to all wavelength channels in a WDM communication systems. We proposed a novel optical ADM and demonstrated the basic functions of individually routing 16 different wavelength channels with 100-GHz channel spacing [23]. The waveguide configuration of 16ch optical ADM is shown in Fig. 13. It consists of four arrayed-waveguide gratings and 16 double-gate TO switches. Four AWGs are allocated with crossing their slab regions each other. These AWGs have the same grating parameters; they are, the channel spacing of 100 GHz and the free spectral range of 3300 GHz (26.4 nm) at 1.55μm region. Equally spaced WDM signals, λ_1, $\lambda_2,\cdots$, λ_{16} , which are coupled to the main input port (add port) in Fig. 13 are first demultiplexed by the AWG_1 (AWG_2) and then 16 signals are introduced into the lefthand-side arms (righthand-side arms) of double-gate TO switches. The cross angle of the intersecting waveguides are designed to be larger than 30 degrees so as to make the crosstalk and insertion loss negligible. Any optical signal coupled into the double-gate TO switch passes through the cross port of one of the four Mach-Zehnder interferometers (MZIs) before reaching the output port. In the single-stage MZI, the light extinction characteristics of the cross port is much better than that of the through port even when the coupling ratio of directional coupler is deviated from 3 dB. Therefore, the crosstalk of double-gate switch becomes substantially improved than that of the conventional single-stage TO switch. We designate here the "off" state of double-gate switch as the switching condition where signal from left input port (right input port) goes to right output port (left output port). The "on" state is then designated as the condition where signal from left input port (right input port) goes to left output port (right output port). When double-gate switch is "off", the demultiplexed light by AWG_1 (AWG_2) goes to the cross arm and multiplexed again by the AWG_3 (AWG_4). On the other hand, if double-gate switch is "on" state the demultiplexed light by AWG_1 (AWG_2) goes to the through arm and multiplexed by the AWG_4 (AWG_3). Therefore, any specific wavelength signal can be extracted from the main output port and led to the drop port by changing the corresponding switch condition. A signal at the same wavelength as that of the dropped component can be added to the main output port

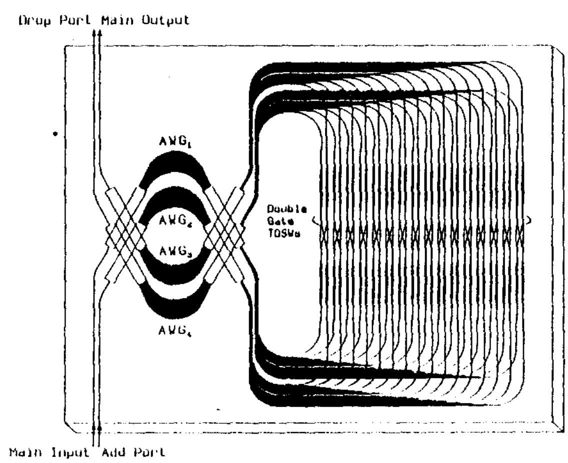

Fig. 13. Waveguide configuration of 16ch optical ADM with double-gate TO switches.

when it is coupled into add port in Fig. 13. When TO switches SW_2, SW_4, SW_6, SW_7, SW_9, SW_{12}, SW_{13} and SW_{15}, for example, are turned to "on" the selected signals λ_2, λ_4, λ_6, λ_7, λ_9, λ_{12}, λ_{13} and λ_{15} are extracted from main output port (solid line) and led to the drop port (dotted line) as shown in Fig. 14. The on-off crosstalk is smaller than -28.4 dB with the on-chip losses of 8~10 dB. Since optical signals pass through both AWG_3 and AWG_4 the crosstalk level here is determined by the crosstalk in the arrayed-waveguides. The present optical ADM can transport all input signals to the succeeding stages without inherent power losses. Therefore, these ADMs are very attractive for all optical WDM routing systems and allow the network to be transparent to signal formats and bit rates.

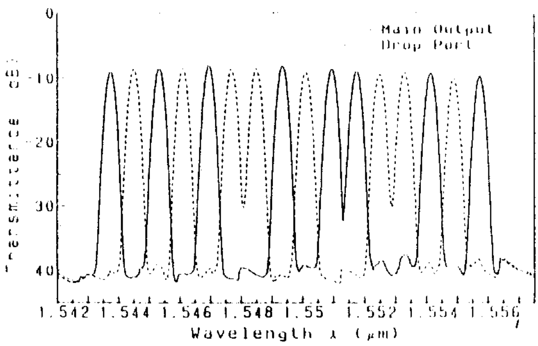

Fig. 14. Transmission spectra from main input port to main output port and drop port when TO switches SW_2, SW_4, SW_6, SW_7, SW_9, SW_{12}, SW_{13}, and SW_{15} are "on".

4. Lattice-Form Programmable Dispersion Equalizers

An advantage of the PLC optical delay equalizer [24],[25] is that variable group-delay characteristics can be achieved by the phase control of silica waveguides. The basic configuration of the PLC delay equalizer is shown in Fig. 15. It consists of nine tunable couplers and eight asymmetrical Mach-Zehnder interferometers cascaded alternately in series. The cross port transfer function of the optical circuit is expressed by a Fourier series as

$$H(z) = \sum_{k=0}^{8} \alpha_k z^{-k+4} \qquad (9)$$

where z denotes $\exp(j2\pi\nu\Delta t)$ (ν : optical frequency, $\Delta t = n_c \Delta L/c$: unit delay time difference in asymmetrical MZ interferometer) and α_k is the complex expansion coefficient. The circuit design procedures are as follows. First the equalizer transfer function to be realized is expressed by the analytical function. Then coefficient α_k's are determined by expanding the analytical function into a Fourier series. Finally coupling ratio (Φ_i) and phase shift value (θ_i) in each stage of lattice filter are determined by the filter synthesis method [26]. In ultrahigh speed optical fiber

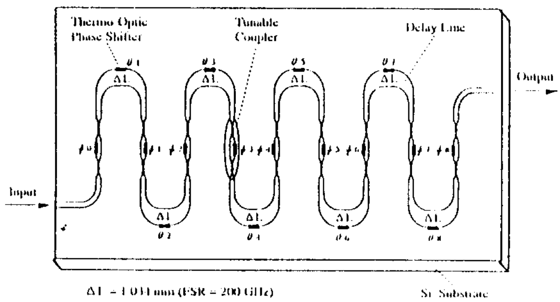

Fig. 15. Basic configuration of the PLC equalizer.

transmission systems (>100 Gbit/s), the effect of the higher order dispersion (third order dispersion or dispersion slope) in the dispersion shifted fiber (DSF) is one of the major factors limiting the transmission distance [27]. Programmable dispersion equalizers can be designed so as to compensate for the higher order dispersion of DSFs. Figure 16(a) shows the measured power transmittance and relative delay time of the PLC higher order dispersion equalizer [28]. The dispersion slope of the equalizer is calculated to be -15.8 ps/nm^2. Figure 16(b) is the relative delay of the 300-km DSF. The dispersion slope of DSF is 0.05~0.06 ps/nm^2. Therefore, the equalizer can compensate the higher order dispersion of ~300-km of DSF. Figure 16(c) shows the relative delay time of 300-km DSF cascaded with the equalizer. The positive dispersion slope of the DSF is almost completely compensated by the PLC equalizer. 200 Gbit/s time-division-multiplexed transmission experiment using a dispersion slope equalizer has been carried out over 100-km fiber length [29]. The pulse distortion caused by the dispersion slope was almost completely recovered, and the power penalty was improved by more than 4 dB.

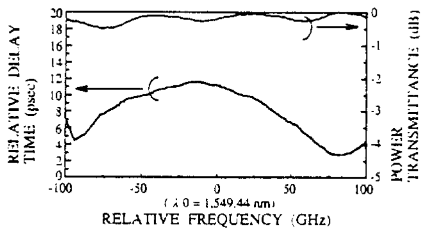

(a) Higher-Order Dispersion Equalizer

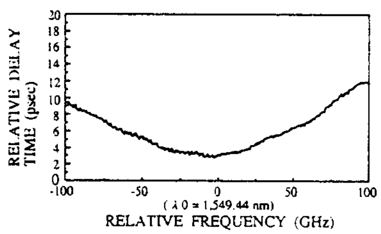

(b) 300-km Dispersion Shifted Fiber

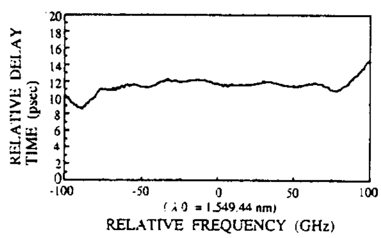

(c) 300-km DSF + Equalizer

Fig. 16. Relative delay times of (a) PLC higher order dispersion equalizer, (b) 300-km DSF and (c) 300-km DSF + equalizer.

5. Hybrid Integration Technology using PLC Platforms

It is widely recognized that optical hybrid integration is potentially a key technology for fabricating advanced integrated optical devices [4]. A silica-based waveguide on a Si substrate is a promising candidate for the hybrid integration platform since high-performance PLCs have already been fabricated using silica-based waveguides and Si has highly stable mechanical and thermal properties which make it suitable as an optical bench. Figure 17 shows the PLC platform fabrication process [30]. First, a thick undercladding is deposited on a Si substrate with a terraced region using FHD, and then the surface of the substrate is flattened by mechanical polishing. To minimize the optical coupling loss between the opto-electronics (OE) device on the terrace and optical waveguide, a thin layer is deposited on the polished substrate surface. The thickness of the layer corresponds to the height of the active region of OE device on the terrace. Then, a core layer is deposited and patterned into a core ridge by RIE. The core ridge is then covered by the overcladding layer. Finally, RIE is used to form the Si terrace for the OE devices on the PLC and the terrace surface is exposed. The relative positions of the core and Si terrace surface are determined precisely because the terrace acts as an etch-stop layer during the RIE process. As a result, Si terrace functions as both a high-precision alignment plane and heatsink when OE device is flip-chip bonded on the terrace.

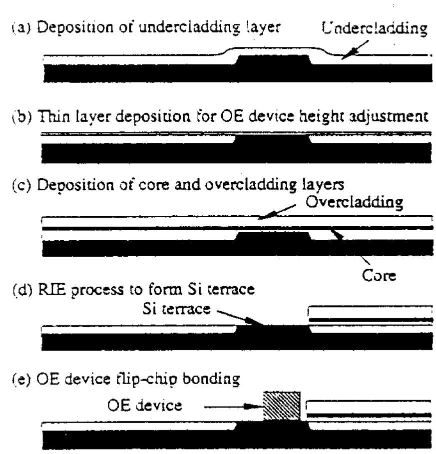

Fig. 17. PLC platform fabrication process.

PLC platform technology has also been utilized in fabrication of a hybrid integrated external cavity laser [31]. Figure 18 shows the configuration of multiwavelength external cavity laser with a uv written grating [32]. Bragg gratings with 2-nm wavelength interval are written into each waveguide by ArF excimar laser irradiation through phasemasks. Figure 19 shows the measured output spectra. Each laser operates in a single longitudinal mode with a side-mode suppression of 40 dB. The temperature sensitivity of the oscillation frequency is -1.7 GHz/degree, which is one eighth of the DFB lasers. Four channel simultaneous modulation experiment has been successfully carried out at 2.5 Gbit/s [33]. Temperature stable multiwavelength source will play an important role in WDM transmission and access network systems.

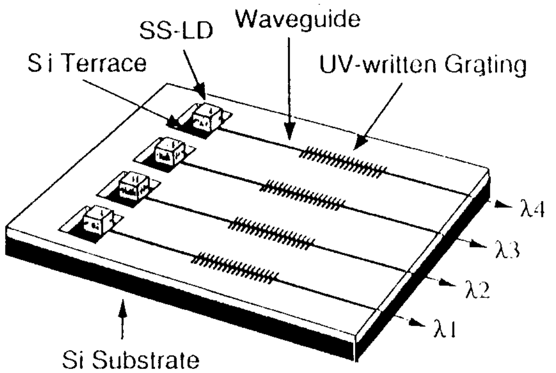

Fig. 18. Configuration of hybrid integrated multi-wavelength external cavity laser.

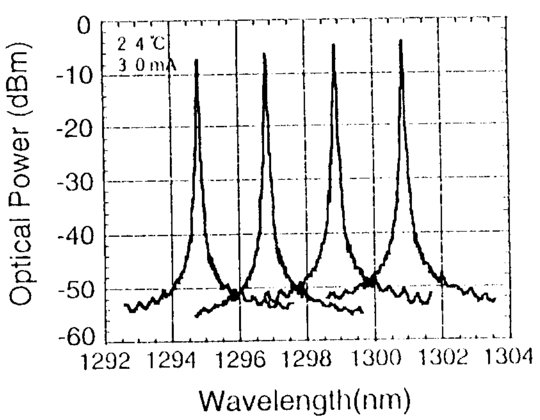

Fig. 19. Oscillation spectra of 4-wavelength laser.

6. Summary

Recent progress in planar lightwave circuits have been reviewed. The PLC technologies supported by continuous improvements in waveguide fabrication, circuit design and device packaging will further proceed to a higher level of integration of optics and electronics aiming at the next generation of telecommunication systems.

Acknowledgments

The authors would like to thank all members in the Photonic Component Laboratory and Okamoto Research Laboratory for their contributions to this work.

References

[1] M.Kawachi, "Silica waveguide on silicon and their application to integrated-optic components", Opt. and Quantum Electron., vol. 22, pp.391-416, 1990.

[2] K.Okamoto, "Planar lightwave circuits (PLCs)", Photonic Networks, Springer-Verlag pp.118-132, 1997.

[3] A.Himeno et al., "System applications of large-scale optical switch matrices using silica-based planar lightwave circuits", Photonic Networks, Springer-Verlag, pp.172-182, 1997.

[4] Y.Yamada et al., "Application of planar lightwave circuit platform to hybrid integrated optical WDM transmitter/receiver module", Electron. Lett., vol. 31, pp.1366-1367, 1995.

[5] Y.Akahori et al., "A hybrid high-speed silica-based planar lightwave circuit platform integrating a laser diode and a driver IC", Proc. IOOC/ECOC '97, Edinburgh UK, vol.2,pp.359-362, 1997.

[6] S.Suzuki et al., "Large-scale and high-density planar lightwave circuits with high-ΔGeO_2-

doped silica waveguides", Electron. Lett., vol. 28, pp.1863-1864, 1992.
[7] Y.Hibino et al., "Propagation loss characteristics of long silica-based optical wave - guides on 5 inch Si wafers", Electron. Lett., vol. 29, pp.1847-1848, 1993.
[8] Y.Hida et al., "10-m long silica-based waveguide with a loss of 1.7 dB/m", IPR'95, Dana Point, CA, 1995.
[9] M.K.Smit, "New focusing and dispersive planar component based on an optical phased array", Electron. Lett., vol. 24, pp.385-386, 1988.
[10] H.Takahashi et al., "Arrayed-waveguide grating for wavelength division multi/demultiplexer with nanometer resolution", Electron. Lett., vol. 26, pp.87-88, 1990.
[11] K.Okamoto et al., "Fabrication of 64x64 arrayed-waveguide grating multiplexer on silicon", Electron. Lett., vol. 31, pp.184-185, 1995.
[12] K.Okamoto et al., "Fabrication of 128-channel arrayed-waveguide grating multiplexer with a 25-GHz channel spacing", Electron. Lett., vol. 32, pp.1474-1476, 1996.
[13] H.Yamada et al., "Statically-phase-compensated 10 GHz-spacing arrayed-waveguide grating", Electron. Lett., vol. 32, pp.1580-1582, 1996.
[14] K.Okamoto et al., "Arrayed-waveguide grating multiplexer with flat spectral response", Opt. Lett., vol. 20, pp.43-45, 1995.
[15] M.R.Amersfoort et al., "Passband broadening of integrated arrayed waveguide filters using multimode interference couplers", Electron. Lett., vol. 32, pp.449-451 , 1996.
[16] D.Trouchetet al., "Passband flattening of PHASAR WDM using input and output star couplers designed with two focal points", Proc. OFC '97 ThM7, Dallas, Texas, 1997.
[17] K.Okamoto et al., "Flat spectral response arrayed-waveguide grating multiplexer with parabolic waveguide horns", Electron. Lett., vol. 32, pp.1661-1662, 1996.
[18] W.K.Burns et al., "Optical waveguide parabolic coupling horns", Appl. Phys. Lett., vol. 30, pp.28-30, 1977.
[19] K.Takada et al., "Measurement of phase error distributions in silica-based arrayed-waveguide grating multiplexers by using Fourier transform spectroscopy", Electron. Lett., vol. 30, pp.1671-1672, 1994.
[20] H.Takahashi et al., "Transmission characteristics of arrayed waveguide NxN wavelength multiplexer", Jour. of Lightwave Tech., vol. 13, pp.447-455, 1996.
[21] O.Ishida et al., "Loss-imbalance equalization in arrayed-waveguide-grating (AWG) multiplexer cascades", J. Lightwave Technol., vol. 13, pp.1155-1163, 1995.
[22] Y.Inoue et al., "Athermal silica-based arrayed-waveguide grating (AWG) multiplexer", IOOC-ECOC '97 postdeadline paper pp.33-36, Edinburgh, UK, 1997.
[23] K.Okamoto et al., "16-channel optical Add/Drop multiplexer consisting of arrayed-waveguide gratings and double-gate switches", Electron. Lett., vol. 32, pp.1471-1472, 1996.
[24] K.Takiguchi et al., "Planar lightwave circuit optical dispersion equalizer", IEEE Photonics Tech. Lett., vol. 6, pp.86-88, 1994.
[25] K.Takiguchi et al., "Dispersion compensation equalizer", Electron. Lett., vol. 31, pp.2192-2193, 1995.
using a variable group-delay dispersion
[26] K.Jinguji et al., "Synthesis of coherent two-port lattice-form optical delay-line circuit", IEEE Jour. Lightwave Tech., vol. 13, pp.73-82, 1995.
[27] S.Kawanishi et al., "200 Gbit/s, 100 km time-division-multiplexed optical transmission using supercontinuum pulses with prescaled PLL timing extraction and all-optical demultiplexing", Electron. Lett., vol. 31, pp.816-817, 1995.
[28 K.Takiguchi et al., "Higher order dispersion equalizer of dispersion shifted fiber using a lattice-form programmable optical filter", Electron. Lett., vol. 32, pp.755-757, 1996.

[29] K.Takiguchi et al., "Dispersion slope equalizing experiment using planar lightwave circuit for 200 Gbit/s time-division-multiplexed transmission", Electron. Lett., vol. 32, pp.2083-2084, 1996.
[30] Y.Yamada et al., "Silica-based optical waveguide on terraced silicon substrate as hybrid integration platform", Electron. Lett., vol. 29, pp.444-445, 1993.
[31] T.Tanaka et al., "Integrated external cavity laser composed of spot-size converted LD and uv written grating in silica waveguide on Si", Electron. Lett., vol. 32, pp.1202-1203, 1996.
[32] T.Tanaka et al., "Fabrication of hybrid integrated 4-wavelength laser composed of uv written waveguide gratings and laser diodes", OECC '97 10D3-3, Seoul, Korea, 1997.
[33] H.Takahashi et al., "A 2.5 Gb/s, 4-channel multiwavelength light source composed of uv written waveguide gratings and laser diodes integrated on Si", IOOC-ECOC '97 pp.355-358, Edinburgh, UK, 1997.

This paper was also published on IEICE Trans. Electron., Vol. E81-C, No.8, pp.1176-1186, August 1998.